

Mean-field theory of the phase diagram of ultrasoft, oppositely charged polyions in solution

Arash Nikoubashman, Jean-Pierre Hansen, and Gerhard Kahl

Citation: *J. Chem. Phys.* **137**, 094905 (2012); doi: 10.1063/1.4748378

View online: <http://dx.doi.org/10.1063/1.4748378>

View Table of Contents: <http://jcp.aip.org/resource/1/JCPSA6/v137/i9>

Published by the [American Institute of Physics](#).

Additional information on *J. Chem. Phys.*

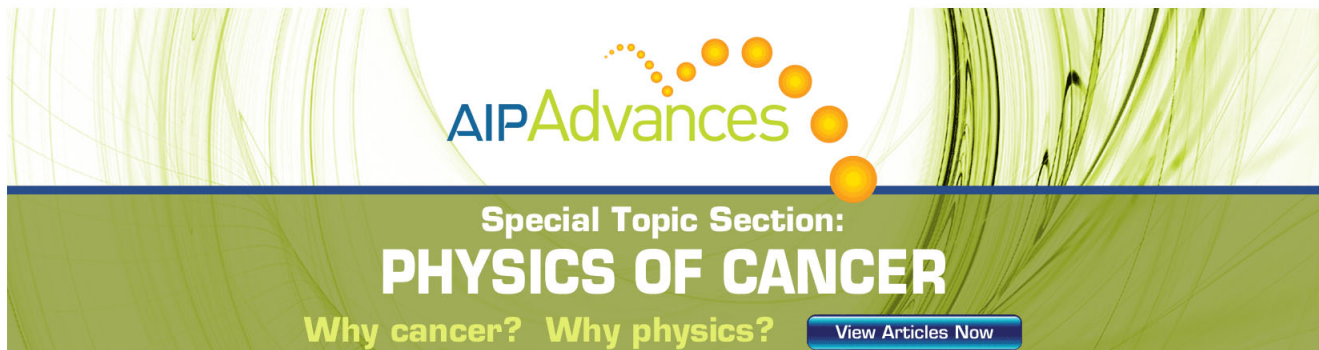
Journal Homepage: <http://jcp.aip.org/>

Journal Information: http://jcp.aip.org/about/about_the_journal

Top downloads: http://jcp.aip.org/features/most_downloaded

Information for Authors: <http://jcp.aip.org/authors>

ADVERTISEMENT



AIPAdvances

Special Topic Section:
PHYSICS OF CANCER

Why cancer? Why physics? [View Articles Now](#)

Mean-field theory of the phase diagram of ultrasoft, oppositely charged polyions in solution

Arash Nikoubashman,^{1,a)} Jean-Pierre Hansen,^{2,3} and Gerhard Kahl¹

¹*Institute of Theoretical Physics and CMS, Vienna University of Technology, Wiedner Hauptstraße 8-10, A-1040 Vienna, Austria*

²*Department of Chemistry, University of Cambridge, Cambridge, United Kingdom*

³*PECSA and CNRS UMR 7195, Université Pierre et Marie Curie, Paris, France*

(Received 17 July 2012; accepted 10 August 2012; published online 7 September 2012)

We investigate the phase separation of the “ultrasoft restricted primitive model” (URPM), a coarse-grained representation of oppositely charged, interpenetrating polyelectrolytes, within a mean-field description based on the “chemical picture.” The latter distinguishes between free ions and dimers of oppositely charged ions (Bjerrum pairs) which are in chemical equilibrium governed by a law of mass action. Interactions between ions, and between ions and dimers are treated within linearized Poisson-Boltzmann theory, at four levels of approximation corresponding to increasingly refined descriptions of the interactions. The URPM is found to phase separate into a dilute phase of dimers, and a concentrated phase of mostly free (unpaired) ions below a critical temperature T_c . The phase diagram differs, however, considerably from the predictions of recent simulations; T_c is about three times higher, and the critical density is much lower than the corresponding simulation data [D. Coslovich, J. P. Hansen, and G. Kahl, *Soft Matter* 7, 1690 (2011)]. Possible reasons for this unexpected failure of mean-field theory are discussed. The Kirkwood line, separating the regimes of monotonically decaying and damped oscillatory decay of the charge-charge correlation function at large distances is determined within the random phase approximation. © 2012 American Institute of Physics. [<http://dx.doi.org/10.1063/1.4748378>]

I. INTRODUCTION

Solutions of oppositely charged polyelectrolyte chains in polar solvents are known to aggregate into neutral or charged polyelectrolyte complexes in the presence or absence of salt, a process referred to as complex coacervation.^{1–4} Theoretical descriptions of polyelectrolyte complexation are usually formulated within a statistical field-theoretic framework,⁵ using perturbation theory,⁶ or computer simulation.⁷ In this paper, we adopt a different approach based on the recognition that, just as for neutral polymers in solution,⁸ swollen polyelectrolyte coils in good solvent can easily interpenetrate. Hence, on the mesoscopic scale of the radius of gyration R_g , swollen polyanions and polycations can be conveniently represented as “ultrasoft” coils interacting *via* effective pair potentials between their centers of mass (CM) which involve a penetrable (“ultrasoft”) core of radius of the order of R_g . In other words, the free energy cost for full overlap of two coils calculated by averaging over all monomer degrees of freedom is typically of the order of a few thermal energy units $k_B T$.^{9,10} This situation contrasts with the hard, impenetrable core of microscopic ions in electrolytes and ionic liquids, or of charged colloidal particles in solution, so-called “colloidal electrolytes.”^{11–13} The standard model used to describe electrolytes is the “primitive model” (PM) of oppositely charged hard spheres in a dielectric continuum of permittivity ϵ representing the polar solvent.¹⁴

Recently, the PM has been generalized to the case of solutions of penetrable polyanions and polycations, referred to as the “ultrasoft primitive model” (UPM).^{15,16} The “restricted” version of the model (i.e., the “ultrasoft restricted primitive model” or URPM), which is symmetric under charge conjugation, was extensively investigated by molecular dynamics (MD) simulations, providing detailed data of the structure, phase behavior, and dynamics of the model over a wide range of temperatures T and polyion densities n .^{15,16} At low T and n , oppositely charged polyions are found to aggregate into neutral, long-lived dimers and, to a lesser extent, tetramers, a behavior reminiscent of that observed earlier for the “restricted primitive model” (RPM).^{17,18} This aggregation leads to a continuous transition between a high temperature and density conducting state, dominated by the free (unpaired) polyions, and a low temperature and density insulating state with a vanishing fraction of unpaired ions. Below a critical temperature T_c , the URPM is found to undergo a first order phase separation between a dense, conducting phase, characterized by a finite ionic conductivity and a divergent dielectric permittivity, coexisting with a dilute insulating phase with vanishing conductivity and finite permittivity. This “liquid-gas” phase coexistence is reminiscent of a similar phase diagram of the RPM of electrolytes,¹⁹ which is by now well characterized thanks to extensive grand-canonical Monte Carlo (MC) simulations combined with a careful finite size scaling analysis.^{20,21} While the critical behavior of the RPM has been clearly identified as being of the Ising universality class,^{21,22} preliminary evidence provided by the MD simulations of the URPM suggests tricritical

^{a)}arash.nikoubashman@tuwien.ac.at.

behavior,^{15,16} yet to be confirmed by a finite size scaling analysis.

In this paper we present a mean-field theory of the phase diagram of the URPM, based on the “chemical picture,” whereby the URPM is treated as a three-component system of free polyanions, free polycations, and neutral, polarizable Bjerrum pairs.²³ The latter are weakly interacting and may hence, in a first approximation, be treated as an ideal gas of fluctuating dimers. The unpaired polyions are treated within linearized Poisson-Boltzmann (i.e., Debye-Hückel) theory¹⁴ adapted to the case of quenched internal polyionic charge distributions spread out over the coil volume $\sim R_g^3$ (rather than mere point charges). In a second step, the interactions between polyions and dimers are included at three levels of approximation corresponding to increasing refinements of the theory. Our approach is closely related to the mean-field description of the RPM, the most advanced version of which achieves nearly quantitative agreement of the calculated phase diagram with the results of MC simulations.²⁴ There are, however, major qualitative differences between the RPM and the URPM. In the former there is an obvious competition between excluded volume effects, due to the hard cores of the ions, and the Coulombic interactions, while the URPM involves only purely Coulombic interactions between spatially extended polyionic charge distributions. Moreover, the presence of impenetrable cores in the RPM implies that the Bjerrum pairs carry permanent dipole moments leading to strong electrostatic interactions between dimers, and between dimers and unpaired ions, while the dimers of the URPM are merely polarizable and hence interact more weakly between themselves and with the polyions compared to the case of the RPM. Despite this apparent simplification, we have found (cf. Sec. V) that the mean-field phase diagram of the URPM agrees poorly with the MC results of Refs. 15 and 16. Possible reasons for this unexpected failure of mean-field theory will be discussed in Sec. VII.

II. THE MODEL

The URPM is a system of $n/2 = N/(2V)$ polycations and as many polyanions per unit volume, carrying opposite charges $\pm Q = \pm Ze$, where e is the proton charge. These charges are smeared over a volume of the order of the cube of their common radius of gyration R_g . More precisely, the normalized charge distribution $w(r)$ associated with each polyion is assumed to be Gaussian, namely,

$$\pm Qw(r) = \pm \frac{Q}{(2\pi\sigma^2)^{3/2}} \exp[-r^2/(2\sigma^2)], \quad (1)$$

where r is the distance from the CM of the coil, and $\sigma \simeq R_g$ will henceforth be chosen to be the length scale. The Fourier transform (FT) of the distribution $w(r)$ is

$$\hat{w}(k) = \int e^{ikr} w(r) dr = \exp[-k^2\sigma^2/2]. \quad (2)$$

The electrostatic potential $\varphi(r)$ generated by the charge distribution (1) is according to Poisson’s equation:

$$\varphi_{\pm}(r) = \frac{\pm Q}{\epsilon r} \operatorname{erf}[r/(\sqrt{2}\sigma)], \quad (3)$$

and the pair potential between an α and a β polyion ($\alpha, \beta = +$ or $-$) is¹⁶

$$v_{\alpha\beta}(r) = \int \varphi_{\alpha}(r') Q_{\beta} w(|\mathbf{r} - \mathbf{r}'|) d\mathbf{r}' = \frac{Q_{\alpha} Q_{\beta}}{\epsilon r} \operatorname{erf}[r/(2\sigma)]. \quad (4)$$

In Eqs. (3) and (4), ϵ is the dielectric permittivity of the implicit solvent.

For $r \gg \sigma$, the pair potentials (4) go over to the Coulombic pair potential between point ions, $Q_{\alpha} Q_{\beta}/(\epsilon r)$, while for $r \rightarrow 0$, i.e., for two overlapping polyions, $v_{\alpha\beta}(r)$ remains finite

$$v_{\alpha\beta} \underset{r \rightarrow 0}{\simeq} u_{\alpha\beta} \left[1 - \frac{r^2}{12\sigma^2} + \frac{r^4}{160\sigma^4} - \mathcal{O}(r^6) \right], \quad (5)$$

where

$$u_{\alpha\beta} = \frac{Q_{\alpha} Q_{\beta}}{\sqrt{\pi} \epsilon \sigma} = \pm u_0. \quad (6)$$

$u_0 = Q^2/(\sqrt{\pi} \epsilon \sigma)$ will henceforth be chosen as the energy scale. The FT of Eq. (4) is

$$\hat{v}_{\alpha\beta}(k) = \frac{4\pi Q_{\alpha} Q_{\beta}}{\epsilon k^2} \exp[-k^2\sigma^2]. \quad (7)$$

Note that since $v_{\alpha\beta}(r = 0)$ is finite, there is no “Coulomb collapse” between oppositely charged polyions, a direct consequence of the extended ionic charge distribution (1).

The classical ground state energy of the system (corresponding to the $T \rightarrow 0$ limit of the internal energy) is¹⁶

$$u(T = 0) = -\frac{N}{2} u_0. \quad (8)$$

This energy is extensive, so that the URPM is thermodynamically stable according to Ruelle’s stability criterion.²⁵ The pair structure of the URPM is characterized in r -space by the pair correlation functions $h_{++}(r) = h_{--}(r)$ and $h_{+-}(r)$, and in k -space by the structure factors $S_{++}(k) = S_{--}(k)$ and $S_{+-}(k)$, where

$$S_{\alpha\beta}(k) = \frac{1}{2} \delta_{\alpha\beta} + \frac{n}{4} \hat{h}_{\alpha\beta}(k). \quad (9)$$

These correlation functions give access to the thermodynamic properties of the URPM *via* the standard energy, virial, and compressibility routes;¹⁶ we will briefly return to the asymptotic behavior of these correlation functions in Sec. VI, but they will only play an implicit role in the mean-field analysis of the URPM phase diagram presented in Secs III-V.

Throughout the remainder of this paper, reduced units will be employed for all relevant physical variables, thus

$$x = r/\sigma ; q = k\sigma ; n^* = n\sigma^3 ; T^* = k_B T/u_0. \quad (10)$$

In particular

$$\frac{v_{\alpha\beta}(r)}{k_B T} = \pm \frac{\sqrt{\pi}}{T^*} \frac{\operatorname{erf}(x/2)}{x} \underset{x \rightarrow 0}{\simeq} \pm \frac{1}{T^*} \left[1 - \frac{x^2}{12} + \mathcal{O}(x^4) \right]. \quad (11)$$

For convenience, the stars will be dropped in what follows, i.e., the systematic use of reduced units will be assumed throughout.

III. THE “CHEMICAL PICTURE”

Due to the pronounced tendency towards polyion aggregation (essentially anion/cation pairing) revealed by the MD simulations of the URPM at low T and small n ,^{15,16} the traditional fluid integral equations for the pair structure, such as the random phase approximation (RPA), or the hyper-netted-chain equation break down in that regime and fail to predict the phase separation observed in the simulations. To account explicitly for the dominant polyion pairing, we hence adopt the “chemical picture” which proved so successful in the case of the RPM.^{24,26} This three-component picture assumes that there exists a chemical equilibrium between free polycations and polyanions, and long-lived Bjerrum pairs. Let $n_1 = n_1^+ + n_1^-$ be the number of free polyions per unit volume and n_2 the number of Bjerrum pairs per unit volume. They are related to the total number n of ions (free and paired) per unit volume by

$$n = n_1 + 2n_2. \quad (12)$$

Charge neutrality obviously implies that $n_1^+ = n_1^- = n_1/2$. The reduced free energy per unit volume $f = F/(Vu_0)$ is a function of T , n_1 , and n_2 , $f = f(T, n_1, n_2)$. The chemical potentials of species 1 (free ions) and 2 (Bjerrum pairs) are given by

$$\mu_1 = \mu_1^+ = \mu_1^- = \left(\frac{\partial f}{\partial n_1} \right)_{T, n_2} \quad (13)$$

$$\mu_2 = \left(\frac{\partial f}{\partial n_2} \right)_{T, n_1}.$$

Chemical equilibrium at constant volume and temperature is achieved when

$$df = \mu_1 dn_1 + \mu_2 dn_2 = 0. \quad (14)$$

Combination of Eqs. (12) and (14) leads to the expected chemical equilibrium condition:

$$\mu_2(T, n_1, n_2) = 2\mu_1(T, n_1, n_2). \quad (15)$$

For a given temperature T and overall ion density n , Eq. (15) determines the fraction of free ions,

$$\alpha = \frac{n_1}{n}. \quad (16)$$

The required free energy density f is conveniently divided into ideal and excess parts:

$$f(T, n_1, n_2) = f_1^{\text{id}}(T, n_1) + f_2^{\text{id}}(T, n_2) + f_{11}^{\text{ex}}(T, n_1, n_2) + f_{12}^{\text{ex}}(T, n_1, n_2) + f_{22}^{\text{ex}}(T, n_1, n_2). \quad (17)$$

The ideal contributions of the free ions and of the Bjerrum pairs (dimers) are given by the standard expressions,

$$f_1^{\text{id}} = n_1 T \left[\ln \left(\frac{n_1}{2} \right) - 1 \right], \quad (18a)$$

$$f_2^{\text{id}} = n_2 T \left[\ln \left(\frac{n_2}{\xi^3} \right) - 1 \right], \quad (18b)$$

where ξ^3 is the dimensionless internal configurational partition function of a Bjerrum pair:

$$\xi^3 = 4\pi \int_0^X \exp \left[-\frac{1}{T} v_{+-}(x) \right] x^2 dx. \quad (19)$$

Here, $x = r/\sigma$ is the distance between the CMs of the paired anion and cation, while $X = R/\sigma$ denotes the cut-off distance, the choice of which is somewhat arbitrary. Different criteria for X and its dependence on T and/or n_1 are discussed, along with the ensuing consequences on some physical properties, in Appendix A.

The excess part f^{ex} of the free energy density in Eq. (17) splits into three contributions arising from the polyion-polyion interactions (f_{11}^{ex}), from polyion-dimer interactions (f_{12}^{ex}), and from dimer-dimer interactions (f_{22}^{ex}) which will be calculated in Sec. IV within mean-field theory. The chemical potentials are calculated from Eqs. (13), (17), and (18):

$$\begin{aligned} \mu_1(T, n_1, n_2) &= \mu_1^{\text{id}}(T, n_1) + \mu_1^{\text{ex}}(T, n_1, n_2) \\ &= T \ln \left(\frac{n_1}{2} \right) + \left(\frac{\partial f^{\text{ex}}(T, n_1, n_2)}{\partial n_1} \right)_{T, n_2}, \end{aligned} \quad (20a)$$

$$\mu_2(T, n_1, n_2) = T \ln \left(\frac{n_2}{\xi^3} \right) + \left(\frac{\partial f^{\text{ex}}(T, n_1, n_2)}{\partial n_2} \right)_{T, n_1}. \quad (20b)$$

Substitution of the expressions (20) in the equilibrium conditions (15) leads to the following law of mass action:

$$\begin{aligned} \frac{n_2}{n_1^2} &= K(T, n_1, n_2) \\ &= \frac{\xi^3}{4} \exp \left\{ \frac{1}{T} [2\mu_1^{\text{ex}}(T, n_1, n_2) - \mu_2^{\text{ex}}(T, n_1, n_2)] \right\}, \end{aligned} \quad (21)$$

where $K(T, n_1, n_2)$ is the equilibrium constant explicitly given by the right-hand side of Eq. (21), provided approximate expressions for μ_1^{ex} and μ_2^{ex} are available (cf. Sec. IV).

In the following we will also need the (reduced) electric polarizability ζ of a Bjerrum pair which determines the electric dipole induced by an external electric field. Within linear response

$$\zeta = \frac{\sqrt{\pi}}{3T} \langle x^2 \rangle, \quad (22)$$

where the thermal average is taken with the weight function (A1). For its actual calculation (involving again the cut-off distance X) we refer to Appendix A.

IV. MEAN-FIELD THEORY: FOUR LEVELS OF APPROXIMATION

This section focuses on the calculation of the excess contribution f_{11}^{ex} and f_{12}^{ex} to the free energy density (17). The contribution f_{22}^{ex} will be neglected throughout, since the electrostatic interactions between neutral, polarizable Bjerrum pairs are expected to be very weak in the absence of permanent dipole moments (which are present in the case of the RPM), particularly at low temperatures. In Ref. 16 it was shown that

the van der Waals dipole-induced dipole interaction between two polarizable Bjerrum pairs is much weaker than the ion-induced dipole interaction, which will be included at approximation level D. We have adopted four levels of approximation (labeled by A to D) corresponding to increasing refinements of the mean-field theory of the URPM.

Level A: At the lowest level, polyion pairing is completely ignored, i.e., all polyions are assumed to be free. Under those conditions, $n_2 = 0$ and $n_1 = n$ whatever the temperature. The only non-zero contributions to the free energy density (17) are f_1^{id} , given by Eq. (18a), and $f_{11}^{\text{ex}}(T, n)$. The excess solvation free energy is calculated within the mean-field Poisson-Boltzmann (PB) theory¹⁴ adapted to extended polyions. Let a polyion α of charge Q_α ($\alpha = +$ or $-$) be pinned at the origin. If $\rho_+^\alpha(x)$ and $\rho_-^\alpha(x)$ are the spherically symmetric local densities of polycations and polyanions building up around the central polyion, the total charge density around that ion is

$$Q\rho_c^\alpha(x) = Q \int [\rho_+^\alpha(x') - \rho_-^\alpha(x')] w(|\mathbf{x} - \mathbf{x}'|) d\mathbf{x}' + Q_\alpha w(x), \quad (23)$$

which includes the internal charge density of the central ion itself. The dimensionless electrostatic potential $\Phi_\alpha(x) = Q\Psi_\alpha(x)/(k_B T)$ satisfies Poisson's equation,

$$\nabla_x^2 \Phi_\alpha(x) = -4\pi \lambda_B \rho_c^\alpha(x), \quad (24)$$

where $\lambda_B = Q^2/(\epsilon k_B T \sigma) = \sqrt{\pi}/T$ is the reduced Bjerrum length. To obtain a closed equation for the potential Φ_α , we make the usual Boltzmann mean-field assumption, namely, that

$$\rho_\pm^\alpha(x) = \frac{n}{2} \exp \left[\mp \int \Phi_\alpha(x') w(|\mathbf{x} - \mathbf{x}'|) d\mathbf{x}' \right]. \quad (25)$$

Linearization of the Boltzmann factor (linearized PB, or Debye-Hückel theory) and substitution in Eqs. (23) and (24) leads to the linearized Poisson-Boltzmann (LPB) equation,

$$\begin{aligned} \nabla_x^2 \Phi_\alpha(x) &= -4\pi \lambda_B z_\alpha w(x) \\ &+ q_D^2 \int d\mathbf{x}' \int d\mathbf{x}'' w(|\mathbf{x} - \mathbf{x}'|) w(|\mathbf{x}' - \mathbf{x}''|) \Phi_\alpha(x''), \end{aligned} \quad (26)$$

where $z_\alpha = Z_\alpha/Z$, and $q_D^2 = \kappa_D^2 \sigma^2 = 4\pi^{3/2} n/T$ is the square of the reduced Debye wavenumber κ_D . Taking Fourier transforms of both sides of Eq. (26) and invoking the convolution theorem, one arrives at

$$\hat{\Phi}_\alpha(q) = \frac{4\pi z_\alpha \lambda_B \hat{w}(q)}{q^2 + q_D^2 \hat{w}^2(q)}. \quad (27)$$

The total excess free energy is finally calculated using the Debye charging process.¹⁴ Let $\Phi_j'(x; \lambda)$ be the mean electrostatic potential around polyion j when all charges are scaled by a factor $0 \leq \lambda \leq 1$ to λQ_j , minus the ‘‘self’’ potential due to the

scaled internal charge density of ion j , then

$$\begin{aligned} \frac{F^{\text{ex}}}{k_B T} &= \sum_j z_j \int_0^1 d\lambda \int w_j(x) \Phi_j'(x; \lambda) d\mathbf{x} \\ &= \frac{1}{(2\pi)^3} \sum_j z_j \int_0^1 d\lambda \int \hat{w}_j(q) \hat{\Phi}_j'(q; \lambda) d\mathbf{q}. \end{aligned} \quad (28)$$

Substituting the LBP result (27) (from which the trivial self contribution must be subtracted) in Eq. (28), one arrives at the required result,

$$f_{11}^{\text{ex}} = \frac{F^{\text{ex}} \sigma^3}{V u_0} = -\frac{q_D^2 T}{(2\pi)^2} \int_0^\infty \left[e^{-q^2} + \frac{q^2}{q_D^2} \ln \left(\frac{q^2}{q^2 + q_D^2 e^{-q^2}} \right) \right] dq. \quad (29)$$

As expected, this result is identical to that obtained by a simple RPA closure of the coupled Ornstein-Zernike relations for the URPM.¹⁶ The resulting free energy density

$$f(T, n) = f^{\text{id}}(T, n) + f_{11}^{\text{ex}}(T, n) \quad (30)$$

is easily shown to be a convex function of density for all temperatures, such that there is no phase separation at this level of approximation (‘‘level A’’) contrary to the case of the RPM, where phase separation is predicted at the corresponding (DH) level of approximation.^{19,24,26}

Level B: The next step is to account for ideal Bjerrum pairs, which do not interact among themselves and with the free polyions. The free energy density consequently contains three contributions

$$f = f_1^{\text{id}}(T, n_1) + f_2^{\text{id}}(T, n_2) + f_{11}^{\text{ex}}(T, n_1), \quad (31)$$

given by Eqs. (18) and (29) (where n is replaced by n_1). For a given overall ion density n , n_1 , and n_2 are determined by the law of mass action (21). As will be shown in Sec. V, the ‘‘level B’’ approximation does lead to phase separation.

Level C: At the following level of approximation, the polarizability ζ of the Bjerrum pairs is explicitly taken into account, by calculating the solvation free energy of a polyion in a bath of non-interacting free polyions and polarizable Bjerrum pairs:

$$f = f_1^{\text{id}}(T, n_1) + f_2^{\text{id}}(T, n_2) + f_{11}^{\text{ex}}(T, n_1, n_2). \quad (32)$$

f_{11}^{ex} now depends explicitly both on n_1 and n_2 . The calculation of the solvation free energy f_{11}^{ex} closely follows that of $f_{11}^{\text{ex}}(T, n_1)$ sketched under level A (where Bjerrum pairs were ignored), and is detailed in Appendix B, leading to the result

$$\begin{aligned} f_{11}^{\text{ex}}(T, n_1, n_2) &= -\frac{q_D^2 T}{(2\pi)^2} \int_0^\infty \left[e^{-q^2} + \frac{q^2}{q_D^2} \ln \left(\frac{\chi q^2}{\chi q^2 + q_D^2 e^{-q^2}} \right) \right] dq, \end{aligned} \quad (33)$$

where $\chi = 1 + 4\pi \zeta n_2$ and ζ is the polarizability (22) of a Bjerrum pair. Note that, depending on the choice of cut-off X (discussed in Appendix A), ζ depends either only on T , or on T and n_1 . Here, the square of the reduced Debye wavenumber reads $q_D^2 = 4\pi^{3/2} n_1/T$.

Level D: As a final refinement of the theory, we take into account the interaction between free polyions and Bjerrum pairs, by adding the solvation free energy f_{12}^{ex} of a Bjerrum

pair in a bath of non-interacting free polyions, leading to a total free energy density

$$f = f_1^{\text{id}}(T, n_1) + f_2^{\text{id}}(T, n_2) + f_{11}^{\text{ex}}(T, n_1, n_2) + f_{12}^{\text{ex}}(T, n_1, n_2). \quad (34)$$

The calculation of f_{12}^{ex} is detailed in Appendix C, with the result

$$f_{12}^{\text{ex}}(T, n_1, n_2) = -\frac{2n_2}{\sqrt{\pi}} \int_0^\infty (1 - e^{-3Tq^2}) \times \left[e^{-q^2} + \frac{q^2}{q_D^2} \ln \left(\frac{q^2}{q^2 + q_D^2 e^{-q^2}} \right) \right] dq. \quad (35)$$

Numerical results for various properties including phase diagrams, based on approximation levels B, C, and D are presented in Sec. V.

V. RESULTS

Before presenting detailed numerical results for the “chemical equilibrium” between free polyions and Bjerrum pairs as functions of T and n , and of the resulting phase diagrams, we briefly return to the determination of the cut-off distance $X(T, n_1)$ of Bjerrum pairs introduced in Appendix A. According to Eq. (25), the PB result for the density $\rho_-^+(x)$ of anions around a central cation (identical to the density $\rho_+^-(x)$ of cations around a central anion) is given by

$$\rho_-^+(x) = \frac{n_1}{2} \exp[u_-^+(x)/T], \quad (36)$$

where $u_-^+(x)/T = \int \Phi_+(x') w(|\mathbf{x} - \mathbf{x}'|) d\mathbf{x}'$. The Fourier transform $\hat{u}_-^+(q)$ is calculated *via* the convolution theorem using Eq. (2) and the reduced potential $\hat{\Phi}_\alpha(q)$ given in Eq. (27). The resulting $u_-^+(x)/T$ obtained by inverse Fourier transformation of $\hat{u}_-^+(q)$ is obviously an approximation, since we have not solved the nonlinear PB equation, but allows us to obtain a reasonable estimate of the cut-off distance $X(T, n_1)$. Examples of $u_-^+(x)/T$ for two free ion densities n_1 and several temperatures are shown in Figure 1. The (approximate) argument of the Boltzmann factor is seen to be quite large at small x , particularly at low T and n_1 , and linearization is only justified for $x > X(T, n_1)$, i.e., when $u_-^+(x)/T < 1$.

We now turn to the “chemical equilibrium” between free (unpaired) polyions and dimers (Bjerrum pairs), governed by the law of mass action (21). Let $\alpha = n_1/n$ be the fraction of monomers (free ions). We have calculated α as a function of T along two isochores ($n = 0.0035$ and $n = 0.01$) and as a function of n along two isotherms ($T = 0.02$ and $T = 0.04$) within mean-field approximation levels B, C, and D, using both cut-offs $X = X(T)$ and $X = X(T, n_1)$. The results turn out to be remarkably insensitive to the choice of cut-off, and the curves shown in Figures 2(a)-3(b) all correspond to the latter choice [$X = X(T, n_1)$].

Along isochores [Figures 2(a) and 2(b)] one would expect $\alpha \rightarrow 1$ at high temperatures, where Bjerrum pairs break up. α is indeed found to be vanishingly small at low T and to increase rapidly beyond $T \simeq 0.04$ (for $n = 0.0035$) and

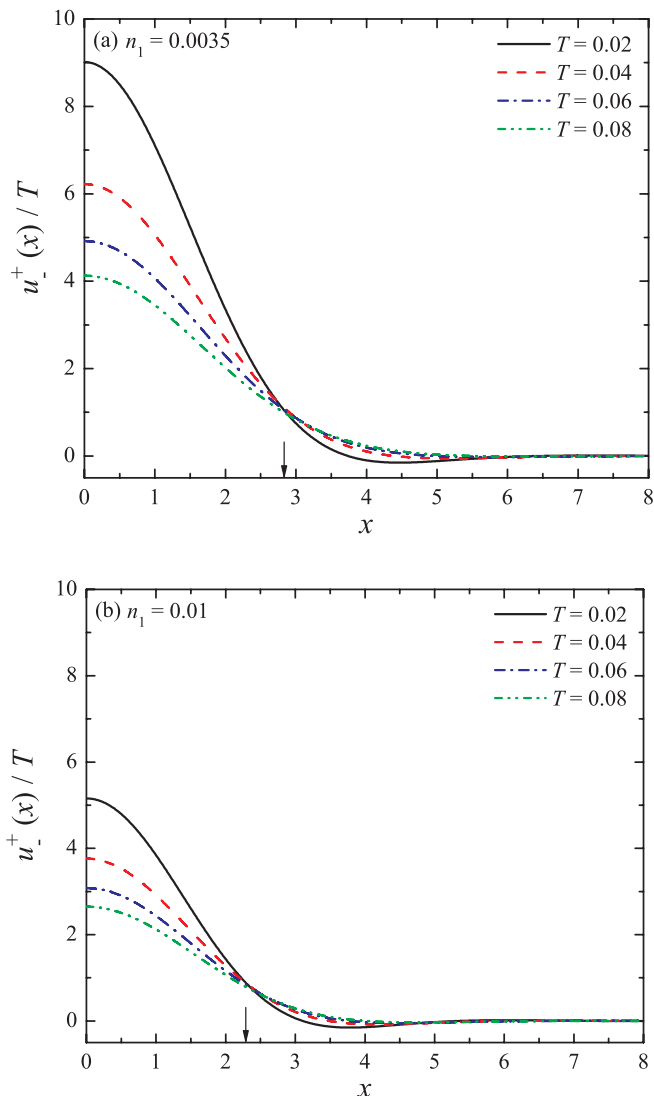


FIG. 1. $u_-^+(x)/T$ vs. x for $T = 0.02, 0.04, 0.06$, and 0.08 (from top to bottom), and $n_1 = 0.0035$ (panel a) and $n_2 = 0.01$ (panel b). The arrows along the x -axis indicate the position of the cut-off distance $X(T, n)$ for $T = 0.02$.

$T \simeq 0.02$ (for $n = 0.01$). There are significant quantitative differences between the predictions based on approximation level B (which entirely neglects any coupling between monomers and dimers), and the more advanced approximation levels C and D which lead to rather similar results. A similar observation holds for the variation of α with n along isotherms, shown in Figures 3(a) and 3(b). At the lower temperatures, the variation of α with n is nearly discontinuous within approximation level B, while it is smoother when ion-pair coupling is included (levels C and D). Along the isochores, α does not saturate towards 1 as T increases, and similarly no saturation is observed along the isotherms upon increasing the density as one would have expected. This lack of saturation towards fully “ionized” states at high T or n may be attributed to the ambiguity in the distinction between Bjerrum pairs and free (unpaired) ions, also encountered in the MD simulations of Ref. 16. In any case, the curves shown in Figures 2(a)-3(b) point to a transition between insulating states, where all polyions are paired, at low T and n , and conducting (ionic) states, dominated by unpaired polyions, at

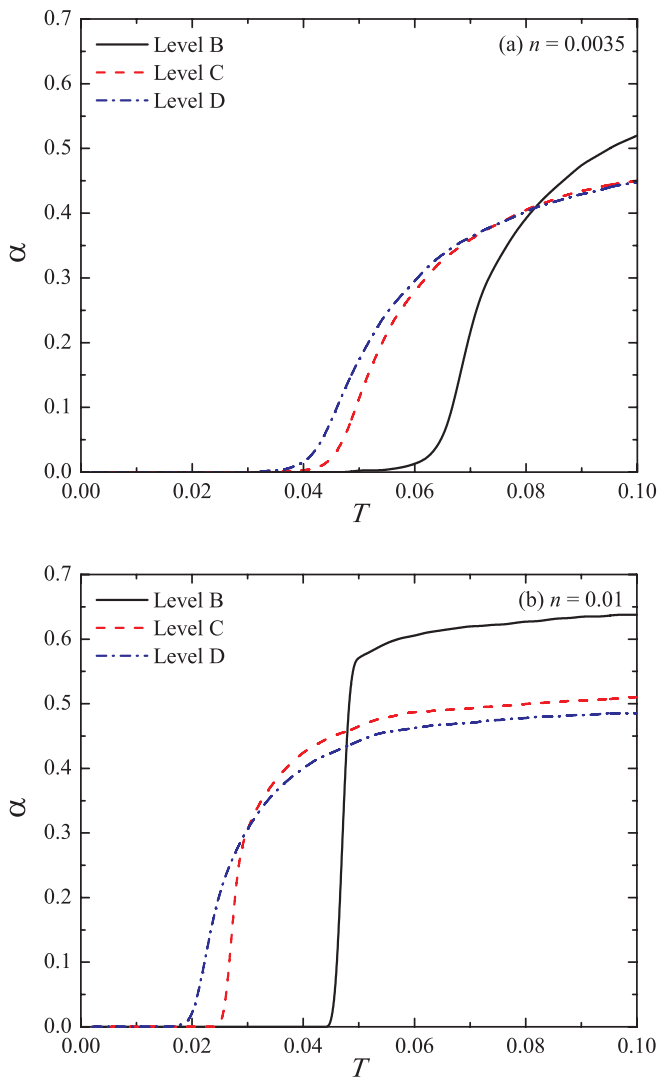


FIG. 2. Fraction α of free ions vs. temperature T along the isochore $n = 0.0035$ (panel a) and $n = 0.01$ (panel b) calculated within approximation levels B, C, and D.

high T and n . As shown by the MD simulations of Refs. 15 and 16, such a transition is associated with a first order phase separation between a low density phase and a high density “liquid” phase below a critical (or tri-critical) temperature T_c .

We have determined the phase coexistence line within the present mean-field framework, by minimizing the grand potential density $\omega(T, \mu_1, \mu_2) = \Omega/V$ with respect to the number densities n_1 and n_2 of free ions and Bjerrum pairs. Chemical equilibrium implies $\mu_1 = 2\mu_2$ [cf. Eq. (15)], so that we are left with minimizing

$$\omega(T, \mu_1, 2\mu_1) = \min_{n_1, n_2} [f(T, n_1, n_2) - \mu_1(n_1 + 2n_2)] \quad (37)$$

for fixed values of T and μ_1 . Equation (37) determines the overall ion densities of the coexisting phases below T_c . The resulting phase diagrams, calculated within the levels of approximation B, C, and D, are shown in Figure 4 and compared to the MD predictions of Refs. 15 and 16; the corresponding critical parameters T_c , n_c , P_c , and $Z_c = P_c/(T_c n_c)$ are listed in Table I.

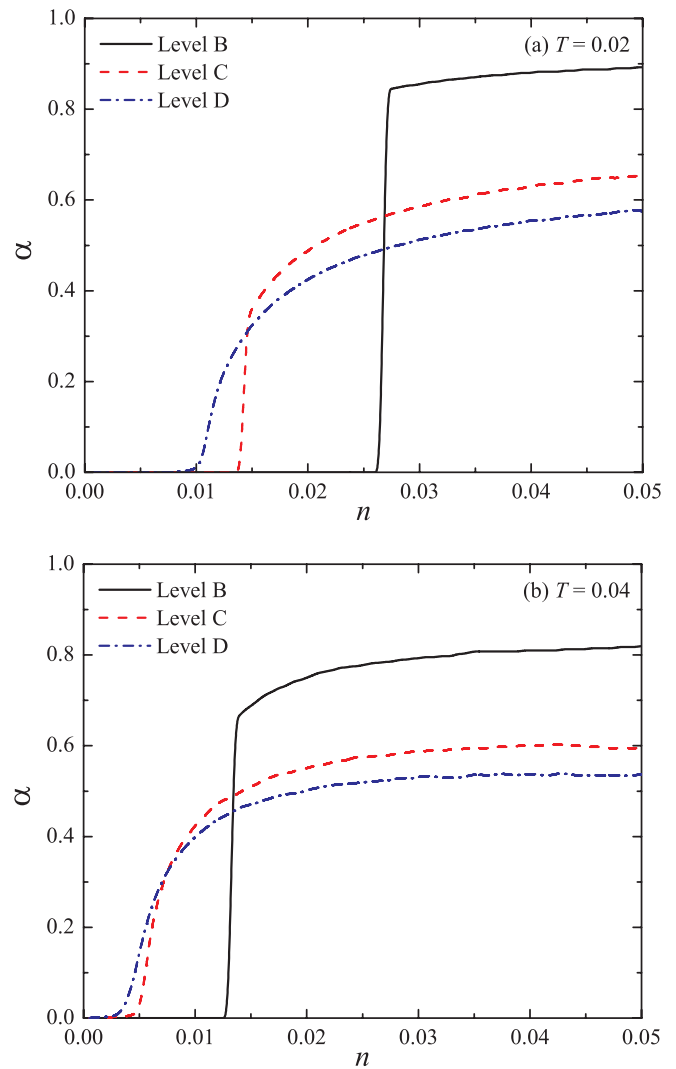


FIG. 3. Fraction α of free ions vs. total ion density n along the isotherms $T = 0.02$ (panel a) and $T = 0.04$ (panel b).

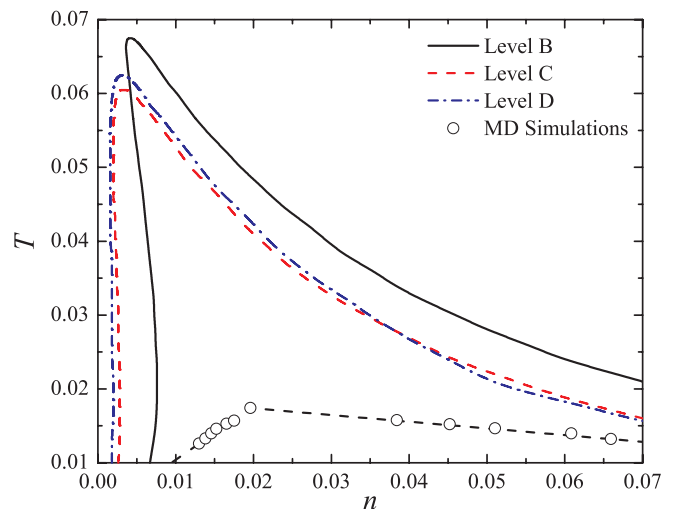


FIG. 4. Phase diagrams of the URPM in the (n, T) plane from approximation levels B, C, and D, and from MD simulations.^{15,16}

TABLE I. Critical temperature T_c , density n_c , pressure P_c , and osmotic coefficient Z_c , estimated from approximations B, C, and D, and from MD simulations.^{15,16}

Model	T_c	n_c	P_c	Z_c
B	0.0675 ± 0.0005	0.0042 ± 0.0001	1.12×10^{-4}	0.395
C	0.0605 ± 0.0005	0.0033 ± 0.0001	5.07×10^{-5}	0.254
D	0.0625 ± 0.0005	0.0032 ± 0.0001	4.31×10^{-5}	0.216
MD	0.0180 ± 0.0002	0.0200 ± 0.0002	2×10^{-4}	0.556

While the three levels of mean-field theory lead to reasonably similar phase diagrams, they differ considerably from the MD results: the critical temperatures are roughly three times higher than the MD prediction, while the critical density n_c is far too low. The very shape of the mean-field coexistence curves differs qualitatively from the MD curve, since the density n_v of the vapor phase increases with decreasing temperature. While the MD results point to tri-critical behavior at T_c (with a critical exponent $\beta = 1$), the mean-field predictions are compatible with classical van der Waals behavior ($\beta = 0.5$). Possible reasons for this somewhat surprising quantitative and qualitative failure of mean-field theory of the URPM will be discussed in Sec. VII.

VI. THE KIRKWOOD LINE

In ionic fluids, the charge-charge correlation function $h_{cc}(r)$ exhibits, at high enough concentration or density, marked oscillatory behavior as a function of ion-ion distance r , associated with “charge ordering” which ensures local electro-neutrality, while at low ion concentration the charge-charge correlations tend to decay monotonically. The so-called “Kirkwood line” is the locus of points in the (n, T) plane where the asymptotic decay of $h_{cc}(r)$ crosses over from monotonic to damped oscillatory at large r .²⁷ The Kirkwood line for the RPM has been determined on the basis of the analytic solution of the mean-spherical approximation (MSA)²⁸ for the model of oppositely charged hard spheres.²⁹ In the case of the RPM, the charge ordering at high densities results from an optimal alternation of shells of anions and cations around a central ion, which allows local charge neutrality to be enforced under the excluded volume constraint. In the case of the URPM, the latter constraint no longer applies, since oppositely charged ions may now overlap, which allows different spatial arrangements of ions to achieve local charge neutrality. Nevertheless, we show in this section that a well-defined Kirkwood line exists for the URPM, at least within the framework of the RPA, which is the equivalent of the MSA for the RPM. In the absence of hard cores, the RPA closure relation reduces to

$$c_{\alpha\beta}(x) = -\frac{v_{\alpha\beta}(x)}{T} = \mp \frac{\sqrt{\pi}}{T} \operatorname{erf}(x/2), \quad (38)$$

where $\alpha, \beta = +$ or $-$, $c_{\alpha\beta}(x)$ is the direct correlation function for $\alpha\beta$ pairs, and the pair potentials given by Eq. (4). Together with the Ornstein-Zernike relations linking the direct and total correlation functions $c_{\alpha\beta}(x)$ and $h_{\alpha\beta}(x)$, the closure relations (38) form a closed set which is easily solved in Fourier space,

leading to the result^{15,16}

$$\hat{h}_{\alpha\beta}(q) = -\frac{4\pi z_{\alpha} z_{\beta} \lambda_B e^{-q^2}}{q^2 + q_D^2 e^{-q^2}}, \quad (39)$$

which implies $h_{++}(x) = h_{--}(x) = -h_{+-}(x)$; the charge-charge correlation function reduces to

$$\hat{h}_{cc}(q) = \hat{h}_{++}(q) - \hat{h}_{+-}(q) = -2\hat{h}_{+-}(q) = -\frac{8\pi \lambda_B e^{-q^2}}{q^2 + q_D^2 e^{-q^2}}. \quad (40)$$

$h_{+-}(x)$, and hence $h_{cc}(x)$, follows by inverse Fourier transformation:

$$x h_{+-}(x) = \frac{1}{4\pi^2 n i} \int_{-\infty}^{\infty} e^{iqx} \frac{q_D^2 e^{-q^2}}{q^2 + q_D^2 e^{-q^2}} q dq. \quad (41)$$

The integral can be calculated by contour integration in the complex $q = q_1 + iq_2$ plane. The poles of the integrand in the upper half plane ($q_2 > 0$) correspond to the complex zeros of the denominator

$$q^2 + q_D^2 e^{-q^2} = 0. \quad (42)$$

Separating the real and imaginary parts of Eq. (42), we obtain the following coupled equations for the real and imaginary parts q_1 and q_2 of the zeros:

$$(q_1^2 - q_2^2) + 2q_D^2 e^{-(q_1^2 - q_2^2)} \cos(2q_1 q_2) = 0, \quad (43a)$$

$$2q_1 q_2 - q_D^2 e^{-(q_1^2 - q_2^2)} \sin(2q_1 q_2) = 0. \quad (43b)$$

Purely imaginary poles ($q_1 = 0$) are determined by

$$q_2^2 = q_D^2 e^{q_2^2}. \quad (44)$$

Note that for $q_D^2 > e^{-1}$, Eq. (44) no longer admits a solution, so that there are no purely imaginary poles above that threshold. In the low density limit, $q_D^2 \rightarrow 0$, Eq. (44) admits two roots, $q_2^{(1)} \rightarrow 0$ and $q_2^{(2)} \rightarrow \infty$. As q_D^2 increases, $q_2^{(1)}$ increases, while $q_2^{(2)}$ decreases, and the two roots approach each other along the imaginary axis and finally merge when $q_D^2 = e^{-1}$.

Applying the residue theorem to the right-hand side of Eq. (41), one arrives at the following asymptotic expression for $h_{+-}(x)$:

$$h_{+-}(x) = \frac{1}{2\pi n x} [A(q_2^{(1)}) e^{-q_2^{(1)} x} + A(q_2^{(2)}) e^{-q_2^{(2)} x}], \quad (45)$$

where the amplitudes A are given by

$$A(q_2) = \frac{q_D^2 \exp(q_2^2)}{2[q_D^2 \exp(q_2^2) - 1]}, \quad (46)$$

with $q_2 = q_2^{(1)}$ or $q_2^{(2)}$. In the weak screening limit, $q_D \ll 1$, $q_2^{(1)} \simeq q_D$, while $q_2^{(2)} \gg q_D$, so that the dominant contribution at large distances is given by the pole $q_2^{(1)}$ closest to the real axis, and the asymptotic decay of $h_{+-}(x)$ [and hence of $h_{cc}(x)$] is governed by the Debye screening length $\lambda_D = 1/q_D$, as expected. Eqs. (43a) and (43b) also admit complex pairs of poles

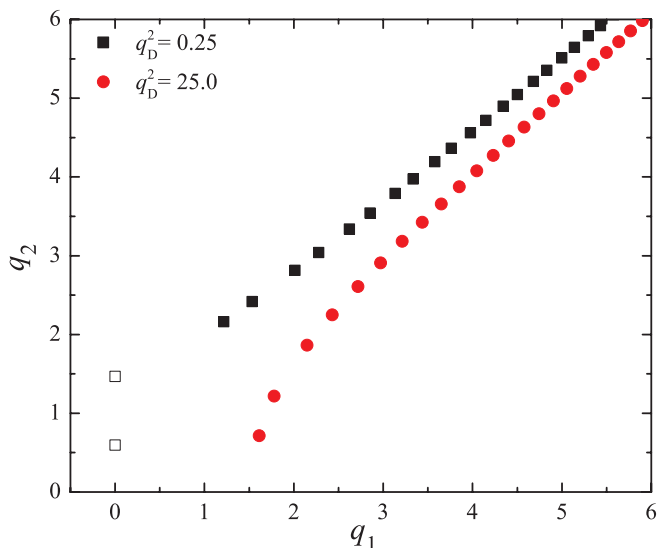


FIG. 5. Positions of purely imaginary poles (open symbols), and of complex poles (filled symbols) in the (q_1, q_2) plane (upper right quadrant) for a low value of $q_D^2 = 0.25$ and a large value of $q_D^2 = 25.0$.

$q = \pm q_1 + iq_2$. Setting $y = 2q_1q_2$ and $z = q_1^2 - q_2^2$, the solutions are of the form

$$y = \pm \sqrt{q_D^4 e^{-2z} - z^2}, \quad (47a)$$

$$z = -q_D^2 e^{-z} \cos\left(\sqrt{q_D^4 e^{-2z} - z^2}\right), \quad (47b)$$

which must be calculated numerically for given q_D^2 . The asymptotic behavior of $h_{+-}(x)$ resulting from the complex pair of poles $q^{(1)} = \pm q_1^{(1)} + iq_2^{(2)}$ with the lowest imaginary part $q_2^{(1)}$ is given by

$$h_{+-}(x) = \frac{1}{2\pi n x} \left[A(q_+^{(1)}) \exp(-q_2^{(1)}x + iq_1^{(1)}x) + A(q_-^{(1)}) \exp(-q_2^{(1)}x - iq_1^{(1)}x) \right], \quad (48)$$

where the amplitudes $A(q_{\pm}^{(1)})$ are defined by

$$A(q) = \frac{q_D^2}{2[\exp(q^2) - q_D^2]}. \quad (49)$$

Figure 5 shows the positions of the purely imaginary and the complex poles in the (q_1, q_2) plane for two values of q_D^2 . In the weak screening case, $q_D^2 = 0.25$, the pole closest to the real axis is the purely imaginary pole with $q_2 = 0.598$. In the strong screening case, $q_D^2 = 25.0$, the pole closest to the real axis is a complex pole $q_1 + iq_2$. In the former case, the asymptotic decay of $h_{+-}(x)$ is monotonic, as in Eq. (45), while in the latter case the asymptotic decay is damped oscillatory as in Eq. (48). The crossover between the two asymptotic decays occurs when the imaginary part q_2 of the complex pair of poles coincides with the position of the purely imaginary pole. The locus of these crossover points defines the Kirkwood line which is mapped out by varying q_D . Examples of the full $h_{+-}(x)$ functions [as calculated by numerical calculation of the Fourier transform (41)], and of the corresponding asymptotic limits are shown in Figure 6 for states

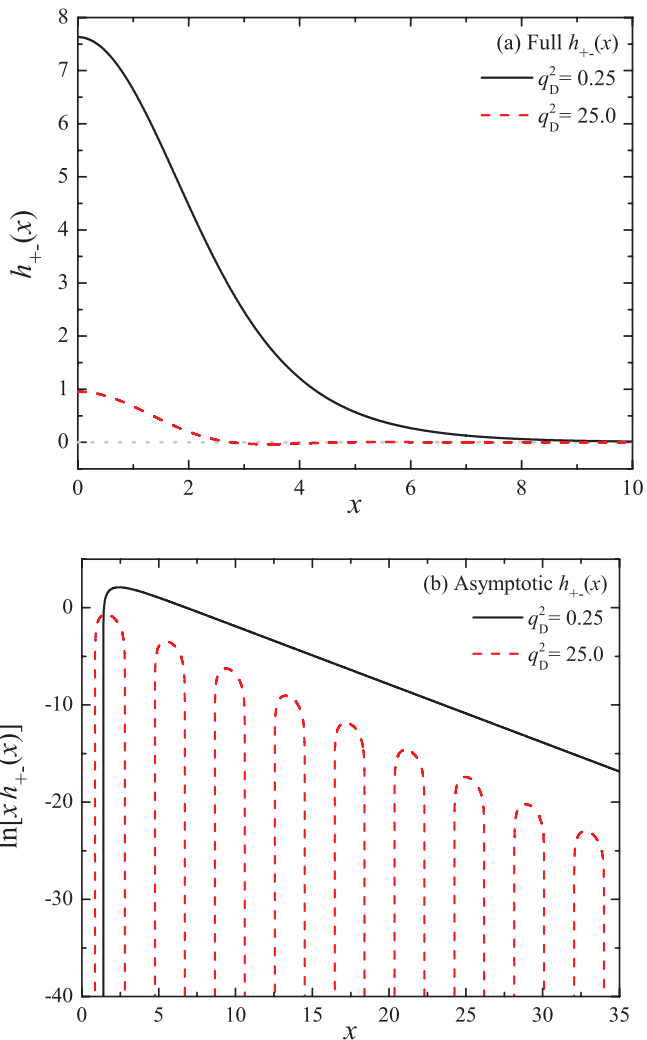


FIG. 6. Full $h_{+-}(x)$ (panel a), and its asymptotic limit (45) (panel b) as a function of x for two cases: one state in the monotonic regime (low q_D^2), and one state in the damped oscillatory regime (high q_D^2). Note that for low q_D^2 the logarithmic plot $\ln[xh_{+-}(x)]$ is a straight line for large x , indicating pure exponential decay at longest range, whereas for high q_D^2 exponentially damped oscillations persist for all distances x .

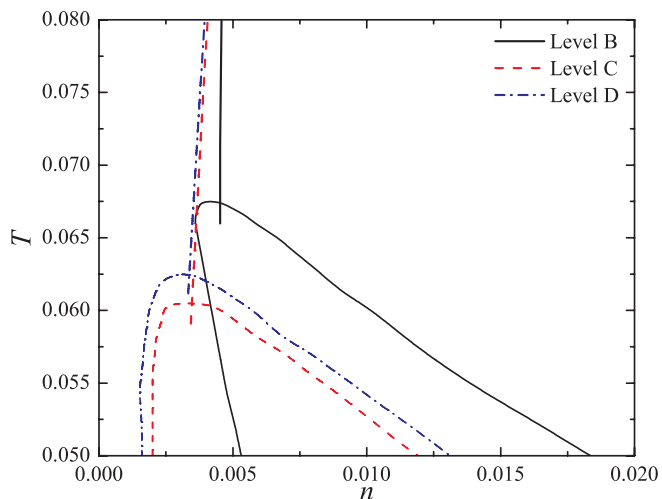


FIG. 7. Kirkwood line in the (n, T) plane, relative to the approximate phase diagram of the URPM.

on both sides of the Kirkwood line, while the position of the Kirkwood line in the (n, T) plane relative to the phase diagram is shown in Figure 7. It is interesting to note that the Kirkwood line intersects the mean-field coexistence curve to the high density side of the critical point. Note that for each thermodynamic state (n, T) , the RPA calculations of $h_{+-}(x)$ and of its asymptotic behavior pertain to the free ions, i.e., correspond to the density $n_1 < n$ of unpaired ions, as calculated from the law of mass action (21).

VII. DISCUSSION AND CONCLUSIONS

We have presented a mean-field description of the phase diagram of the URPM of oppositely charged poly-electrolytes, within the framework of the “chemical picture,” which distinguishes between free polyions and Bjerrum pairs of oppositely charged polyions, and LPB theory to account for ion-ion and ion-pair interactions. Four levels of approximation were investigated, corresponding to progressive refinements of the mean-field formulation. If the formation of Bjerrum pairs is ignored (level of approximation A), LBP theory is equivalent to the RPA, and no phase separation is predicted for the URPM. Approximation levels B, C, and D (defined in Sec. IV) all lead to a phase transition between a low density phase of Bjerrum pairs, and a high density phase of mostly free polyions, below a critical temperature T_c . The phase diagrams predicted by the three levels of approximation are reasonably close, with similar values of T_c , but the critical density n_c shifts to lower densities upon going from approximation level B (which neglects ion-pair couplings) to approximation levels C and D. These findings imply that, since Bjerrum pair formation is included in the theory, the mean-field description is fairly insensitive to the degree to which ion-pair coupling is accounted for. This trend may be traced back to the fact that the neutral Bjerrum pairs, which form at low T and n , are polarizable entities, but do not carry any permanent dipole moments, contrary to the case of the RPM. Consequently, ion-pair and pair-pair interactions are, *a priori*, much weaker in the case of the URPM, compared to the RPM, where they play a very significant role.^{24,26}

The most important, and unexpected conclusion to be drawn from our calculations is the quantitative and even qualitative failure of mean-field theory to predict a phase diagram of the URPM in reasonable agreement with available simulation data,^{15,16} as shown in Figure 4 and Table I. Mean-field theory predicts a far too high critical temperature T_c , and a far too low critical density n_c . Moreover, the critical behavior near the critical point is predicted to be classical van der Waals-like, while the simulations point to possible tri-critical behavior. This strong disagreement between mean-field predictions and simulations is in sharp contrast to the case of the RPM, where nearly quantitative agreement between mean-field theory^{24,26} and Monte Carlo simulations^{20–22} has been found, except in the immediate vicinity of the critical point, where mean-field theory predicts classical critical exponents as opposed to the exponents of the Ising universality class within a proper finite size scaling analysis.

For three-dimensional systems obeying classical statistical mechanics and undergoing a first-order phase transition

which terminates at a critical point, such as the liquid-gas transition of atomic or molecular fluids, or demixing transitions in multi-component fluids, mean-field theory generally provides a quantitatively reasonable estimate of the phase diagram, except in the critical region. It is hence important to analyze possible reasons for the break-down of the theory in the case of the URPM. Some such reasons come immediately to mind:

- (a) The linearization of the Boltzmann factor in Eq. (25), which leads to the LPB equation (26), is obviously not justified when polyions overlap, as illustrated in Figure 1. This shortcoming is, however, at least partly resolved by the introduction of Bjerrum pairs which provide a quantitatively more accurate description of the interaction between strongly overlapping anions and cations. Calculations based on full nonlinear PB theory (discarding Bjerrum pairs as a separate species) are feasible, and planned in future work to resolve this issue.
- (b) The introduction of a neutral species of Bjerrum pairs within the “chemical picture” leads to the possibility of some double-counting of Coulombic interactions between oppositely charged polyions, since the mean-field calculation of the solvation energy of free (unpaired) ions includes contributions from distances less than the cut-off distance, X , defining Bjerrum pairs. However, the insensitivity of the calculated free energy densities to the choice of cut-off indicates that such double-counting is likely to be insignificant.
- (c) The “chemical picture” adopted in this paper allows only for free ions and Bjerrum pairs, while the MD simulations of the URPM^{15,16} point to the existence of non-negligible fractions of higher-order clusters, mostly neutral tetramers. The inclusion of tetramers in the mean-field description would be a highly non-trivial task,¹⁷ but the success of a chemical description involving only Bjerrum dimers in the related case of the RPM^{24,26} gives good reason to believe that the inclusion of higher-order clusters would not change the predictions of mean-field theory drastically.
- (d) A far more plausible reason of the inadequacy of mean-field theory lies in the very specific nature of the URPM. While most standard models undergoing liquid-vapor-like transitions, including the RPM, the van der Waals fluid, the lattice gas, and the isomorphic Ising model, involve a competition between excluded volume (or single occupancy) constraints and nearest neighbor or long-range attractions between particles, the URPM involves only purely Coulombic, attractive or repulsive interactions, with a strong propensity to full overlap of oppositely charged polyions. The “natural” competition between entropic and energetic contributions to the free energy is thus much less clear-cut than in the above-mentioned models, in particular the RPM. Moreover, the ion-pair and pair-pair interactions are of a many-body inductive nature, and hence strongly fluctuating. They are correctly accounted for in the MD simulations,^{15,16} but cannot be properly

described within the chemical picture/mean-field framework.

It is hence plausible that the URPM is fluctuation-dominated over a wide range of thermodynamic states in the (n, T) plane, and not only near criticality. An obvious example of a significant fluctuation mechanism is the formation and break-up of Bjerrum pairs and higher order clusters, which contribute both to the entropic and energetic components of the free energy. We believe that strong fluctuations which are not captured within mean-field theory, are the fundamental reason for the inadequacy of the latter to provide a reasonable estimate of the phase diagram of the URPM.

ACKNOWLEDGMENTS

We thankfully acknowledge Daniele Coslovich for many helpful discussions and for providing the MD simulation data. This work has been supported by the Marie Curie ITN-COMPLOIDS (Grant Agreement No. 234810), by the Austrian Science Foundation (FWF) under Project No. P19890-N16 and by the Studienstiftung des Deutschen Volkes.

APPENDIX A: CALCULATION OF THE CUT-OFF RADIUS

In this appendix we discuss in detail the choice of the cut-off distance X in the internal partition function (19) of a Bjerrum pair. Figure 8 shows the integrand of ξ^3 :

$$\chi(x) = x^2 \exp\left[-\frac{1}{T}v_{+-}(x)\right] = x^2 \exp\left[\frac{\sqrt{\pi} \operatorname{erf}(x/2)}{T} \frac{x}{x}\right] \quad (\text{A1})$$

for three different temperatures. At sufficiently low T , $\chi(x)$ exhibits a sharp maximum at $X = X_1(T)$ and a shallow minimum at $X = X_2(T) > X_1(T)$. At the lowest temperatures, $v_{+-}(x)$ may be replaced by its harmonic form (11). The po-

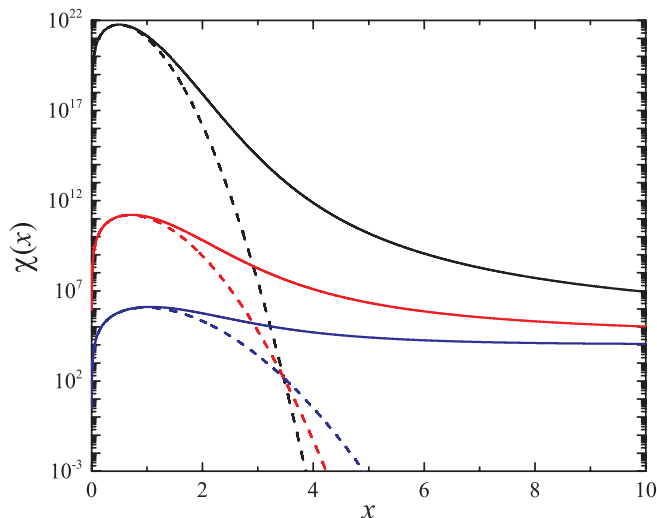


FIG. 8. Integrand $\chi(x)$ of the integral ξ^3 vs. x . Solid lines show the integrand for the exact potential v_{+-} , while the dashed lines show the results for $\chi(x)$ based on the quadratic expansion (11) of $v_{+-}(x)$. Curves are for $T = 0.02$, 0.04, and 0.08 from top to bottom.

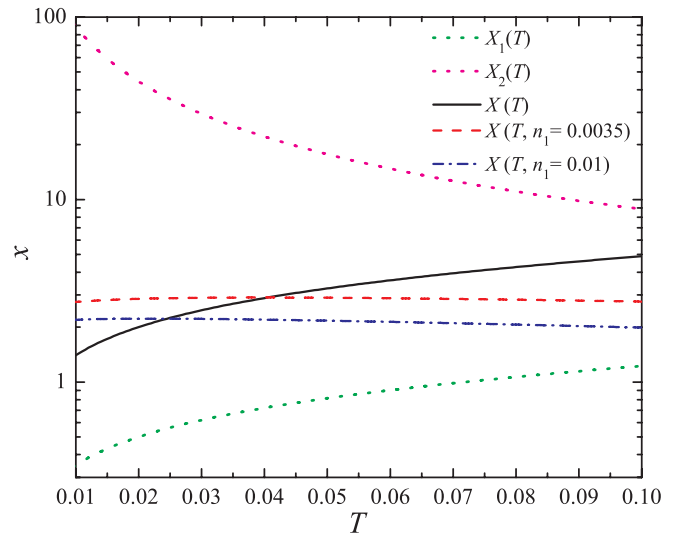


FIG. 9. Positions of the maximum $X_1(T)$ and the minimum $X_2(T)$ of the integrand $\chi(x)$ vs. temperature T , and the cut-off distances $X(T)$, $X(T, n_1 = 0.0035)$, and $X(T, n_1 = 0.01)$ vs. T (see text).

sition of the maximum of $\chi(x)$ is then easily calculated to be

$$X_1(T) = \sqrt{12T} \left[1 + \frac{9}{10}T + \mathcal{O}(T^2) \right]. \quad (\text{A2})$$

On the other hand, since $\operatorname{erf}(x/2) \rightarrow 1$ as $x \rightarrow \infty$, it is easily shown that at low temperatures

$$\lim_{T \rightarrow 0} X_2(T) = \frac{\sqrt{\pi}}{2T} \rightarrow \infty. \quad (\text{A3})$$

As seen in Figure 9, the position of the minimum shifts to lower distances x as T increases. In fact, for $T \gtrsim 0.15$, the minimum disappears and the integrand $\chi(x)$ increases monotonically, signaling that at high temperatures, Bjerrum pairs can no longer be defined, and all polyions behave essentially as free (unpaired) ions.

Following Bjerrum,²³ the usual convention is to choose the cut-off distance in the integral (19) to be $X = X_2(T)$. At low temperatures ($T \ll 0.15$), the position $X_2(T)$ shifts to unphysically large distances [cf., Eq. (A3)], larger than, for instance, the mean distance between polyions $\sim n^{-1/3}$. However, the contribution to the integral (19) from distances beyond two or three times the position of the maximum $X_1(T)$ is practically negligible (except when $T \gtrsim 0.15$), so that we have chosen the operational cut-off $X(T) \simeq 4X_1(T)$. We have verified that the internal partition function ξ^3 is insensitive to this choice, by varying X around this value. In the limit $T \rightarrow 0$, $\xi^3(T)$ may be calculated analytically, by limiting the expansion of $v_{+-}(x)$ to quadratic order in Eq. (11) and letting $X \rightarrow \infty$ [cf., Eq. (A3)] leading to the result

$$\lim_{T \rightarrow 0} \xi^3(T) = \xi_0^3(T) = (12\pi T)^{3/2} e^{1/T}. \quad (\text{A4})$$

The ratio of $\xi_0^3(T)$ over the exact $\xi^3(T)$ is shown in Figure 10 for three different choices of the cut-off distance. As expected, the ratio $\xi_0^3(T)/\xi^3(T) \rightarrow 1$ as $T \rightarrow 0$, and decreases as T increases, because the thermal amplitude of the relative vibration of the anion-cation pairs increases with temperature.

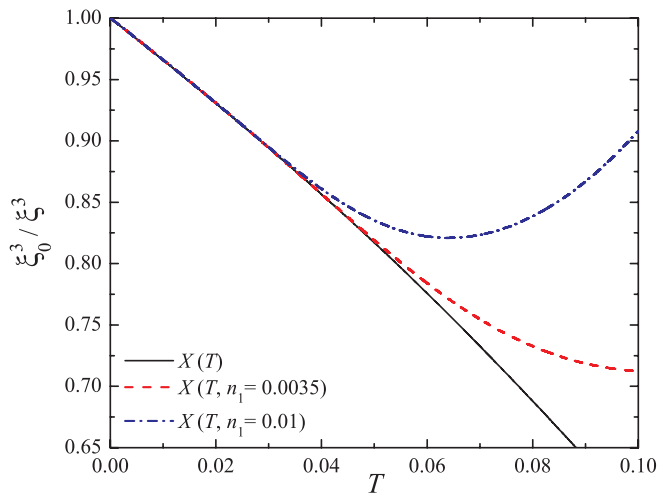


FIG. 10. Ratio ξ_0^3/ξ^3 vs. T for cut-off distances $X(T)$, $X(T, n_1 = 0.0035)$, and $X(T, n_1 = 0.01)$.

We now turn to the actual evaluation of the reduced electric polarizability ζ of a Bjerrum pair as defined by Eq. (22) in the main body of the manuscript. In the harmonic approximation, where $v_{+-}(x)$ is replaced by its quadratic expansion (11), $\langle x^2 \rangle = 18T$, so that $\zeta_0 = 6\sqrt{\pi}$, independent of T . At higher temperatures, $\langle x^2 \rangle$ must be calculated numerically, using the exact expression for $v_{+-}(x)$ and the same cut-off X as used for the internal partition function ξ^3 . As clearly visible in Figure 11, the ratio $\zeta_0/\zeta(T)$ decreases with increasing temperature due to anharmonicity. The Bjerrum pair polarizability will be shown to have a non-negligible effect on f_{11}^{ex} in Secs. IV and V.

So far it has been assumed that the cut-off distance X , and hence the Bjerrum pair partition function ξ^3 and the corresponding polarizability ζ depend only on temperature, which is clearly true at very low densities. At finite densities one may, however, adopt the view that X could also depend on the free ion density n_1 , i.e., $X = X(T, n_1)$, and hence $\xi^3 = \xi^3(T, n_1)$. We have adopted a criterion for the choice of $X(T,$

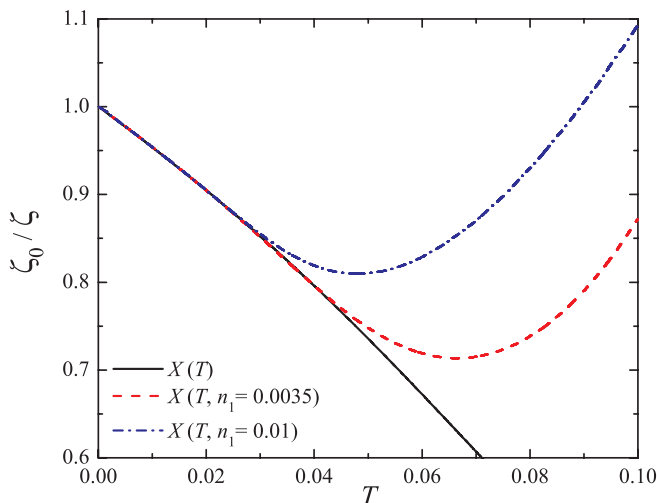


FIG. 11. Ratio ζ_0/ζ of the reduced electric polarizabilities vs. T for cut-off distances $X(T)$, $X(T, n_1 = 0.0035)$, and $X(T, n_1 = 0.01)$.

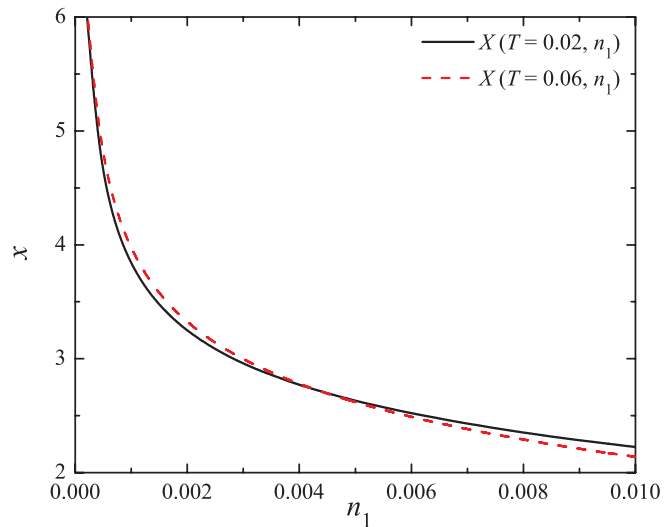


FIG. 12. Cut-off distances $X(T = 0.02, n_1)$ and $X(T = 0.06, n_1)$ vs. n_1 .

$n_1)$ used previously for the two-dimensional Coulomb gas,³⁰ which is intimately linked to the linearization of Poisson-Boltzmann theory for the calculation of the distribution of free polycations around a central polyanion (or conversely), as expounded in the following section. Following the prescription of Ref. 30, the cut-off $X(T, n_1)$ is chosen to be the mean anion-cation distance x below which the argument of the Boltzmann factor (i.e., the screened electrostatic potential divided by $k_B T$) exceeds one, so that linearization is no longer justified. The resulting cut-off distance $X(T, n_1)$ is plotted in Figure 9 as a function of T for two densities n_1 . Compared to $X(T)$, $X(T, n_1)$ hardly varies with T , and drops below $X(T)$ at high temperatures. The resulting ratio $\xi_0^3(T)/\xi^3(T, n_1)$ is shown in Figure 10 as a function of T for the same densities n_1 . Contrary to the ratio $\xi_0^3(T)/\xi^3(T)$, the variation of the former is non-monotonic at higher temperatures, reflecting the effective shrinking of Bjerrum pairs at non-zero free polyion densities n_1 . A similar non-monotonic behavior is observed for the ratio ζ_0/ζ in Figure 11. The n_1 -dependence of $X(T, n_1)$ is shown in Figure 12 for the low density limit, and it is well visible that the cut-off distance increases dramatically as $n_1 \rightarrow 0$. Furthermore, we can clearly see, that $X(T, n_1)$ is rather insensitive to changes in T .

APPENDIX B: SOLVATION ENERGY OF A POLYION IN A BATH OF FREE POLYIONS AND BJERRUM PAIRS

In this appendix we generalize the calculation of the solvation energy of a polyion, presented in Sec. IV, to the case where the central polyion is surrounded by a bath of free polyanions and polycations and of polarizable Bjerrum pairs; the three bath species do not interact (mean-field theory). For the sake of clarity, the central ion is taken to be a cation of charge Q , and we use dimensional variables. The mean charge density around the central cation is given by Eq. (23) (for $\alpha = +$), while the mean polarization density reads

$$\mathbf{P}(\mathbf{r}) = \rho_p(\mathbf{r}) \langle \mathbf{m}(\mathbf{r}) \rangle = -\rho_p(\mathbf{r}) \zeta \nabla \Psi(\mathbf{r}), \quad (\text{B1})$$

where $\rho_p(\mathbf{r})$ is the mean density of Bjerrum pairs, $\langle \mathbf{m}(\mathbf{r}) \rangle$ is the mean dipole moment of a pair induced by the electric field generated by the mean electrostatic potential $\Psi(\mathbf{r})$ around the central ion, and ζ is the Bjerrum pair polarizability given by Eq. (22). The mean electrostatic potential satisfies Poisson's equation,

$$\begin{aligned} \nabla^2 \Psi(\mathbf{r}) &= -\frac{4\pi Q}{\epsilon} \rho_c(\mathbf{r}) + 4\pi \nabla \cdot \mathbf{P}(\mathbf{r}) \\ &= -\frac{4\pi Q}{\epsilon} \left\{ \int w(\mathbf{r}-\mathbf{r}') [\rho_+(\mathbf{r}') - \rho_-(\mathbf{r}')] d\mathbf{r}' + w(\mathbf{r}) \right\} \\ &\quad - 4\pi \zeta \nabla \cdot [\rho_p(\mathbf{r}) \nabla \Psi(\mathbf{r})], \end{aligned} \quad (\text{B2})$$

which generalizes Eq. (24). Within the PB approximation, the local densities $\rho_+(\mathbf{r})$ and $\rho_-(\mathbf{r})$ are given by Eq. (25), while the density of Bjerrum pairs is

$$\rho_p(\mathbf{r}) = n_2 \exp[-\langle \mathbf{m}(\mathbf{r}) \rangle \cdot \nabla \Psi(\mathbf{r}) / (k_B T)]. \quad (\text{B3})$$

Substitution of Eqs. (25) and (B3) in Eq. (B2) leads to the self-consistent PB equation for $\Psi(\mathbf{r})$. The linearized PB equation follows upon linearizing the Boltzmann factors in the right-hand side of the PB equation. Note that linearizing the exponent in Eq. (B3) would still leave a nonlinear term $\sim |\nabla \Psi(\mathbf{r})|^2$. On the other hand, since the coupling between free ions and neutral Bjerrum pairs is expected to be weak, one may reasonably assume that the Bjerrum pairs are uniformly distributed around the central polyion, so that $\rho_p(\mathbf{r})$ may be replaced by the macroscopic density n_2 . The LPB equation thus finally reads

$$\begin{aligned} (1 + 4\pi \zeta n_2) \nabla^2 \Psi(\mathbf{r}) \\ = -\frac{4\pi Q}{\epsilon} w(\mathbf{r}) + \kappa_D^2 \int d\mathbf{r}' \int d\mathbf{r}'' w(\mathbf{r}-\mathbf{r}') w(\mathbf{r}'-\mathbf{r}'') \Psi(\mathbf{r}''). \end{aligned} \quad (\text{B4})$$

Fourier transformation of both sides of Eq. (B4) leads to the result

$$\hat{\Phi}(\mathbf{k}) = \frac{Q \hat{\Psi}(\mathbf{k})}{k_B T} = \frac{4\pi \lambda_B \hat{w}(k)}{k^2 (1 + 4\pi \zeta n_2) + \kappa_D^2 \hat{w}^2(k)}, \quad (\text{B5})$$

which reduces to Eq. (27) if one neglects the polarizability of the Bjerrum pairs ($\zeta = 0$). The electrostatic potential acting on the central ion due to all other ions and Bjerrum pairs follows from Eq. (B5) upon subtracting the ‘‘self potential’’ $4\pi \lambda_B \hat{w}(k)/k^2$ due to the charge distribution of the polycation itself, i.e.,

$$\hat{\Phi}(k) = 4\pi \lambda_B \left[\frac{1}{k^2 (1 + 4\pi \zeta n_2) + \kappa_D^2 \hat{w}(k)} - \frac{1}{k^2} \right] \hat{w}(k). \quad (\text{B6})$$

The total excess free energy of the N_1 free polyions is once more calculated by the Debye charging process

$$F_1^{\text{ex}} = \frac{N_1 Q}{(2\pi)^3} \int_0^1 d\lambda \int \hat{\Psi}(k; \lambda) \hat{w}(k) d\mathbf{k}. \quad (\text{B7})$$

Substituting Eqs. (2) and (B6) in Eq. (B7), integrating over λ and returning to reduced units, one arrives at the required solvation free energy per unit volume, $f_{11}^{\text{ex}} = F_1^{\text{ex}} \sigma^3 / (V u_0)$, quoted in Eq. (33) of the main text. Taking into account the

polarizability of the Bjerrum pairs (approximation level C) leads to the additional factors $\chi = (1 + 4\pi \zeta n_2)$ in the argument of the logarithm, compared to the expression (29) for f_{11}^{ex} obtained by setting $\zeta = 0$ ($\chi = 1$) (approximation level B). The additional factor χ implies that f_{11}^{ex} now depends explicitly both on n_1 and on n_2 .

APPENDIX C: SOLVATION ENERGY OF A BJERRUM PAIR IN A BATH OF FREE POLYIONS

The objective of this appendix is to calculate the contribution f_{12}^{ex} to the excess free energy of the URPM due to ion-pair interactions, within the framework of LPB theory. To this end, we calculate the solvation energy of a single Bjerrum pair in a bath of n_1 non-interacting polyions ($n_1/2$ anions and as many cations). The Bjerrum pair is placed along the z -axis of a Cartesian reference frame with its CM at the origin. Let s be its instantaneous elongation, such that the cation of the pair is placed at $+s\hat{z}/2$ and the anion at $-s\hat{z}/2$ (where \hat{z} is the unit vector along the z -axis). In view of the cylindrical symmetry, the local densities of free polycations and polyanions around the Bjerrum pair are $\rho_+(\mathbf{r}) = \rho_+(r, \theta)$ and $\rho_-(\mathbf{r}) = \rho_-(r, \theta)$, where θ is the polar angle between the position \mathbf{r} of the ion CM and the z -axis. For a given elongation s , the electrostatic potential $\Psi(\mathbf{r}) = \Psi(r, \theta)$ around the Bjerrum pair satisfies Poisson's equation

$$\begin{aligned} \nabla^2 \Psi(\mathbf{r}) &= -\frac{4\pi Q}{\epsilon} \left\{ \int [\rho_+(\mathbf{r}') - \rho_-(\mathbf{r}')] w(|\mathbf{r}-\mathbf{r}'|) d\mathbf{r}' \right. \\ &\quad \left. + \left[w\left(\mathbf{r} - \frac{s}{2}\hat{z}\right) - w\left(\mathbf{r} + \frac{s}{2}\hat{z}\right) \right] \right\}, \end{aligned} \quad (\text{C1})$$

where the second term on the right-hand side is the charge distribution of the Bjerrum pair. The corresponding linearized PB equation reads

$$\begin{aligned} \nabla^2 \Psi(\mathbf{r}) &= \kappa_D^2 \int d\mathbf{r}' \int d\mathbf{r}'' w(\mathbf{r}-\mathbf{r}') w(\mathbf{r}'-\mathbf{r}'') \Psi(\mathbf{r}'') \\ &\quad - \frac{4\pi Q}{\epsilon} \left[w\left(\mathbf{r} - \frac{s}{2}\hat{z}\right) - w\left(\mathbf{r} + \frac{s}{2}\hat{z}\right) \right], \end{aligned} \quad (\text{C2})$$

which generalizes Eq. (26) to the present situation. Taking Fourier transforms of both sides of Eq. (C2), one easily arrives at the following expression for the electrostatic potential:

$$\hat{\Psi}(\mathbf{k}) = \frac{8\pi i Q \sin(sk_z/2) \hat{w}(k)}{\epsilon [k^2 + \kappa_D^2 \hat{w}^2(k)]}, \quad (\text{C3})$$

where $\hat{w}(k)$ is still given by Eq. (2). The solvation energy of the Bjerrum pair of elongation s is once more calculated via the Debye charging process, once the ‘‘self’’ contribution due to the charge distribution of the Bjerrum pair has been duly subtracted from Eq. (C3). Going to polar coordinates in k -space, the result is

$$\begin{aligned} f_2^{\text{ex}}(s) &= -\frac{2Q^2}{\epsilon \pi} \int_0^\infty dk \left[1 - \frac{\sin(sk)}{sk} \right] \\ &\quad \times \left\{ \hat{w}^2(k) - \frac{k^2}{\kappa_D^2} \ln \left[1 + \frac{\kappa_D^2}{k^2} \hat{w}^2(k) \right] \right\}. \end{aligned} \quad (\text{C4})$$

As expected, $f_2^{\text{ex}} \rightarrow 0$ as $s \rightarrow 0$ (i.e., when the two polyions of the Bjerrum pair lie on top of each other), and $f_2^{\text{ex}} \rightarrow 2f_1^{\text{ex}}$

as $s \rightarrow \infty$, where f_1^{ex} is the solvation energy of a single polyion in a bath of polyions [cf., Eq. (29)].

The result (C4) must now be averaged over all values of the elongation s , weighted by the Boltzmann factor $\exp[-\beta v_{+-}(r)]$ for an anion-cation pair. Using the parabolic approximation (5) for $v_{+-}(x)$, and returning to reduced units, the normalized weight function reads

$$p(x)dx = \frac{4\pi x^2}{(\pi X_0)^{3/2}} \exp(-x^2/X_0^2) dx, \quad (\text{C5})$$

where $X_0 = (12T)^{1/2}$ and $x = s/\sigma$. An elementary calculation leads to

$$f_2^{\text{ex}} = -\frac{2}{\sqrt{\pi}} \int_0^\infty dq [1 - \exp(-q^2 X_0^2/4)] \times \left[e^{-q^2} - \frac{q^2}{q_D^2} \ln \left(1 + \frac{q_D^2}{q^2} e^{-q^2} \right) \right]. \quad (\text{C6})$$

The resulting ion-pair contribution to the free energy density, $f_{12}^{\text{ex}} = F_{12}^{\text{ex}}/(Vu_0) = n_2 f_2^{\text{ex}}$ is hence given by Eq. (35) of the main text. Note that f_{12}^{ex} is proportional to the pair density n_2 and depends on n_1 and T through q_D^2 and X_0^2 . The approximate weight function $p(x)$ is valid at low temperature. At higher temperatures, $v_{+-}(x)$ should be replaced by the exact potential (4) and the integration over the reduced anion-cation elongation x must be carried out numerically up to the cut-off distance X introduced in Sec. III.

¹B. Philipp, H. Dautzenberg, K. T. Linov, T. Kötze, and W. Davydoff, *Prog. Polym. Sci.* **14**, 91 (1989).

²E. Tsuchida, *J. Macromol. Sci. Pure Appl. Chem.* **31**, 1 (1994).

³H. Dautzenberg, *Macromolecules* **30**, 7810 (1997).

⁴H. M. Buchhammer, M. Mende, and M. Oelmann, *Colloids Surf., A* **218**, 151 (2003).

⁵G. H. Fredrickson, *The Equilibrium Theory of Inhomogeneous Polymers* (Oxford University Press, New York, 2006).

⁶M. Castelnovo and J. F. Joanny, *Eur. Phys. J. E* **6**, 377 (2001).

⁷J. Lee, Y. O. Popov, and G. H. Fredrickson, *J. Chem. Phys.* **128**, 224908 (2008).

⁸A. Y. Grosberg, P. G. Khalatur, and A. R. Khoklov, *Mater. Chem. Phys.* **3**, 709 (1982).

⁹J. Dautenhahn and C. K. Hall, *Macromolecules* **27**, 5399 (1994).

¹⁰P. G. Bolhuis, A. A. Louis, J. P. Hansen, and E. J. Meijer, *J. Chem. Phys.* **114**, 4296 (2001).

¹¹M. E. Leunissen, C. G. Christova, A. P. Hynninen, C. P. Royall, A. I. Campbell, A. Imhof, M. Dijkstra, R. van Roij, and A. van Blaaderen, *Nature (London)* **437**, 235 (2005).

¹²J. B. Caballero, E. G. Noya, and C. Vega, *J. Chem. Phys.* **127**, 244910 (2007).

¹³E. Sanz, M. E. Leunissen, A. Fortini, A. van Blaaderen, and M. Dijkstra, *J. Phys. Chem. B* **112**, 10861 (2008).

¹⁴D. A. McQuarrie, *Statistical Mechanics* (Harper & Row, New York, 1976).

¹⁵D. Coslovich, J. P. Hansen, and G. Kahl, *Soft Matter* **7**, 1690 (2011).

¹⁶D. Coslovich, J. P. Hansen, and G. Kahl, *J. Chem. Phys.* **134**, 244514 (2011).

¹⁷M. J. Gillan, *Mol. Phys.* **49**, 421 (1983).

¹⁸C. Valeriani, P. J. Camp, J. W. Zwaniikken, R. van Roij, and M. Dijkstra, *Soft Matter* **6**, 2793 (2010).

¹⁹G. Stell, K. C. Wu, and B. Larsen, *Phys. Rev. Lett.* **37**, 1369 (1976).

²⁰A. Z. Panagiotopoulos, *J. Chem. Phys.* **116**, 3007 (2002).

²¹I. M. Caillol, D. Levesque, and J. J. Weis, *J. Chem. Phys.* **116**, 10794 (2002).

²²E. Luijten, M. E. Fisher, and A. Z. Panagiotopoulos, *Phys. Rev. Lett.* **88**, 185701 (2002).

²³N. Bjerrum, *Kgl. Dan. Vidensk. Selsk. Mat.-Fys. Medd.* **7**, 1 (1926).

²⁴M. E. Fisher and Y. Levin, *Phys. Rev. Lett.* **71**, 3826 (1993).

²⁵D. Ruelle, *Statistical Mechanics: Rigorous Results* (World Scientific, Singapore, 1999).

²⁶Y. Levin and M. E. Fisher, *Physica A* **225**, 164 (1996).

²⁷J. G. Kirkwood, *Chem. Rev.* **19**, 275 (1936).

²⁸E. Waisman and J. L. Lebowitz, *J. Chem. Phys.* **56**, 3086 (1972).

²⁹R. J. F. Leote de Carvalho and R. Evans, *Mol. Phys.* **83**, 619 (1994).

³⁰J. P. Hansen and P. Viot, *J. Stat. Phys.* **38**, 823 (1985).